

Angle-dependent reflectivity recovery by planewave synthesis imaging

Jun Ji¹

ABSTRACT

In this paper I compared imaging conditions of three different prestack migrations in terms of angle-dependent reflectivity recovery. The imaging conditions compared are shot profile migration with conventional imaging condition, de Bruijn's imaging condition, and planewave synthesis imaging. The conventional imaging condition can be applied to any reflector geometry and to arbitrary velocity, but it recovers only diagonal component of the reflectivity matrix. de Bruijn's imaging condition recovers full reflectivity matrix but has difficulty in implementing for arbitrary reflector geometry and under variable velocity. Planewave synthesis imaging takes advantages from both conventional and de Bruijn's imaging condition.

INTRODUCTION

During the past decade, the use of AVO (amplitude versus offset) analysis in petroleum exploration has become increasingly common. Even though the goal of AVO analysis is to observe the anomalous angle-dependent reflectivity behavior of a reflector, the name *amplitude versus offset* was chosen because most of the amplitude analysis is done in the common midpoint domain. To analyze the properties of the reflector correctly, we need to know the angle-dependent reflectivity, which is often called AVA (*amplitude versus angle*). When a target reflector is close to horizontal, and velocity does not change much in the lateral direction, angle-dependent reflectivity can be obtained by measuring amplitudes along the offset, followed by ray tracing for each event to determine the corresponding incidence angle to the reflector. If a target reflector has a complex structure and strong lateral velocity variation, however, AVO may not be the same as AVA because the amplitude can be affected not only by the angle-dependent reflectivity but also by wave focusing or defocusing caused by propagation through complex velocities or structures. Resnick et al. (1987) discuss the fact that dips introduce serious problems for AVO analysis. They conclude that performing prestack migration on the data before doing AVO analysis is a necessity. Most present day seismic migration schemes determine only the reflection coefficient of the zero offset or averaged reflectivity over a range of reflection angles for each depth point in the subsurface. This is mainly due to a simplified imaging condition. Recently, de Bruijn et al. (1990) proposed an imaging technique that produces angle-dependent reflectivity. Unfortunately, this scheme is

¹email: jun@sep.stanford.edu

not easy to apply when the reflector is not flat, which commonly happens in the real world. Planewave synthesis imaging (Ji, 1993) is a promising alternative for the angle-dependent reflectivity recovery because it can be applied to any arbitrary structure and implicitly uses the same imaging condition as the one of de Bruin. This paper describes the meaning of the image obtained by planewave synthesis migration. After reviewing the imaging conditions of the conventional prestack migration and of de Bruin et al. (1990), I discuss the equivalence of that of the planewave synthesis imaging. Then I show some examples of angle-dependent reflectivity recovery of each imaging method using synthetic data for comparison.

THE FORWARD MODEL

Since reflectivity imaging is an inversion from seismic data collected at the surface, it is important to understand the implied forward model that relates the reflectivity to surface seismic data. After preprocessing for multiple reflections, the monochromatic 2-D forward model (Berkhout, 1985) for a seismic shot record can be written as follows:

$$\mathbf{g}_j(z_0) = F(z_0, z_0)\mathbf{s}_j(z_0), \quad (1)$$

with

$$F(z_0, z_0) = \sum_{n=1}^N W(z_0, z_n)R(z_n)W(z_n, z_0). \quad (2)$$

In equation (1) source vector $\mathbf{s}_j(z_0)$ and measurement vector $\mathbf{g}_j(z_0)$ refer to one seismic experiment at the surface $z = z_0$ with source location at $x = x_j$. In equation (2), the propagation operators $W(z_n, z_0)$ and $W(z_0, z_n)$ quantify the full propagation effects (down and up, respectively) between depth levels z_0 and z_n , and the reflectivity matrix $R(z_n)$ defines the elastic angle-dependent reflection properties caused by inhomogeneities at depth level z_n . All matrices and vectors refer to one temporal Fourier component. Equations (1) and (2) are valid for single-component as well as multi-component measurement of both 2-D and 3-D data (Berkhout, 1985).

Propagation operators

In order to model seismic data correctly, propagation operator W should be a time extrapolation since wavefield extrapolate in time physically. However, the time extrapolation is not efficient in computation. Instead we use depth extrapolation, which is efficient in computation. If we use depth extrapolation as a propagation operator, however, we cannot model the correct amplitude of the wavefield because the energy of the wavefield in a lossless medium is preserved in time, not in depth. This does not mean that the amplitude of wavefield obtained by depth extrapolation is totally incorrect because most of the energy recorded in reflection seismic travels near the vertical direction and the wavefield becomes a plane wave in the far distance where the energy of the wavefield is preserved both in time and depth. Therefore, if the source wavefield is a plane wave, the amplitude of the wavefield after depth extrapolation behaves similarly to that of the wavefield obtained by time extrapolation.

Reflectivity matrix

The property of the angle-dependent reflectivity matrix $R(z_n)$ in equation (1) becomes clearer if we look at it in the Fourier domain as de Bruin et al. (1990) does. In order to obtain an expression for $R(k_x, z_n, \omega)$, we start with the well-known angle-dependent reflection coefficient $R(z_n, \alpha)$ for two acoustic half-spaces separated by an interface at z_n :

$$R(z_n; \alpha) = \frac{\rho_2 c_2 \cos \alpha - \rho_1 \sqrt{c_1^2 - c_2^2 \sin^2 \alpha}}{\rho_2 c_2 \cos \alpha + \rho_1 \sqrt{c_1^2 - c_2^2 \sin^2 \alpha}}, \quad (3)$$

where c_1 and c_2 are the velocities, ρ_1 and ρ_2 are the mass densities of the upper and lower half-space, respectively, and α is the angle of incidence. By substituting $k_1 = \omega/c_1$, $k_2 = \omega/c_2$, and $k_x = k_1 \sin \alpha$ into equation (3) we obtain

$$R(k_x, z_n, \omega) = \frac{\rho_2 \sqrt{k_1^2 - k_x^2} - \rho_1 \sqrt{k_2^2 - k_x^2}}{\rho_2 \sqrt{k_1^2 - k_x^2} + \rho_1 \sqrt{k_2^2 - k_x^2}}. \quad (4)$$

As an example, Figure 1 shows the angle-dependent reflection coefficients in the (k_x, ω) and (x, ω) domains when $c_1 = 1500\text{m/s}$, $c_2 = 3000\text{m/s}$, $\rho_1 = 1000\text{kg/m}^3$, and $\rho_2 = 1000\text{kg/m}^3$. Since the reflection is a convolution of the downgoing wavefield with the reflection coefficient, the reflectivity matrix in equation (2) can be visualized by taking the reflection coefficient for a given frequency in Figure 1 and making a matrix whose columns are down-shifted reflection coefficients of each other. Figure 2 shows this reflectivity matrix when $\omega = \pi/4$.

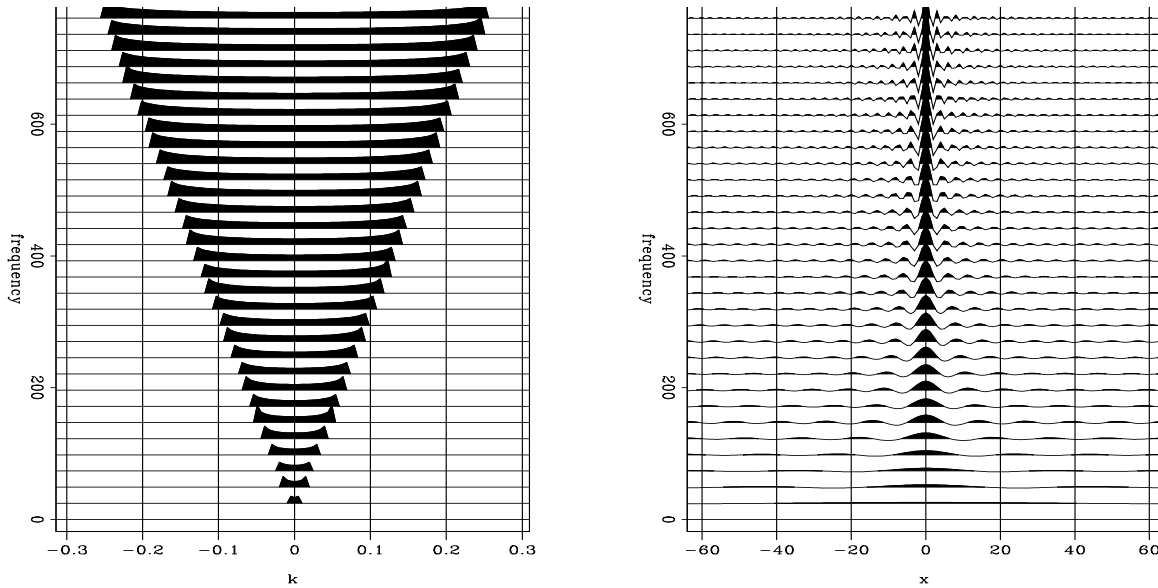
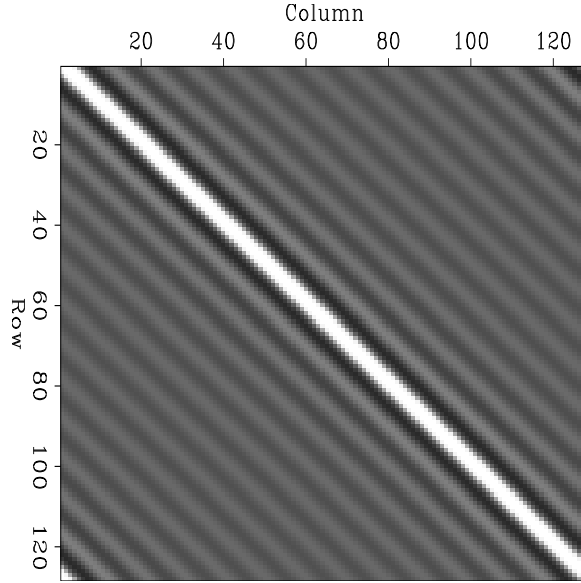


Figure 1: Angle-dependent reflection coefficients in (k_x, ω) (left) and (x, ω) (right) domains when $c_1 = 1500\text{m/s}$, $c_2 = 3000\text{m/s}$, $\rho_1 = 1000\text{kg/m}^3$, and $\rho_2 = 1000\text{kg/m}^3$. jun1-rc-wk-wx
[ER]

Figure 2: Reflectivity matrix R for $\omega = \pi/4$. `jun1-rc-mat` [ER]



REFLECTIVITY IMAGING

For reflectivity imaging, we extrapolate the upcoming and downgoing wavefield recursively for each depth level as follows:

$$\mathbf{g}(z_n) = W^*(z_n, z_m)\mathbf{g}(z_m) \quad (5)$$

and

$$\mathbf{s}(z_n) = W(z_n, z_m)\mathbf{s}(z_m), \quad (6)$$

where $*$ denotes the adjoint and implies that the upcoming waves are extrapolated backward in time; the downgoing waves, forward in time. If we assume that the extrapolation operator is unitary, from the forward model (1) we have

$$\mathbf{g}(z_n) = R(z_n)\mathbf{s}(z_n). \quad (7)$$

Using the above relation, the imaging is performed to retrieve reflectivity matrix $R(z_n)$ from $\mathbf{g}(z_n)$ and $\mathbf{s}(z_n)$ for each depth level. One of the most important properties of the extrapolation operator is the unitary that makes equation (7) true. Even though many algorithms based on the wave equation are accepted as unitary operators, each algorithm has a different property in terms of closeness to unitary. For this paper, I chose the split-step Fourier method (Stoffa and Fokkema, 1990) because of its pseudounitary property (Appendix A).

Conventional prestack imaging

In conventional prestack imaging as in shot profile imaging (Claerbout, 1985), the reflectivity is obtained by deconvolving the downgoing wavefield from the upcoming wavefield in the

(x, ω) domain as follows:

$$X(x, z_n, \omega) = \frac{\mathbf{g}(x, z_n, \omega)\mathbf{s}^*(x, z_n, \omega)}{\mathbf{s}(x, z_n, \omega)\mathbf{s}^*(x, z_n, \omega) + \epsilon^2}, \quad (8)$$

where ϵ^2 represents a small positive value introduced for stability because $\mathbf{s}(x, z_n, \omega)$ may contain zeros. Then imaging is carried out by summation over all frequencies to extract the zero-time component of the reflectivity as follows:

$$R(x, z_n) = \sum_{\omega} X(x, z_n, \omega). \quad (9)$$

Therefore we obtain one reflection coefficient value for each point of the subsurface. Since we performed the deconvolution in the (x, ω) domain by dividing the source wave from received wave in equation (8), we implicitly assumed the reflectivity matrix R is a diagonal matrix. The diagonality of the reflectivity matrix R means locally reacting reflection coefficient. If we assume that source wavefield acts like a planewave locally at reflector, the imaging condition used in the profile imaging will produce the reflection coefficient of the angle that corresponds to the local incidence angle of the source wavefield at each point of the subsurface.

de Bruin's imaging condition

In order to retrieve the full reflectivity matrix, de Bruin et al. (1990) proposes another imaging condition. Instead of deconvolving in the spatial domain, they deconvolve in the Fourier domain (k_x, ω) after Fourier transforming both downgoing and upcoming waves, as follows:

$$X(k_x, z_n, \omega) = \frac{\mathbf{g}(k_x, z_n, \omega)\mathbf{s}^*(k_x, z_n, \omega)}{\mathbf{s}(k_x, z_n, \omega)\mathbf{s}^*(k_x, z_n, \omega) + \epsilon^2}. \quad (10)$$

The next step is to transform $X(k_x, z_n)$ into $X(p, z_n)$ by replacing the wavenumber k_x with the ray parameter $p = k_x/\omega$. Then imaging is carried out in the $p - \omega$ domain along the lines of the constant p :

$$R(p, z_n) = \sum_{\omega} X(p, z_n, \omega). \quad (11)$$

This imaging condition retrieve the full angle-dependent reflectivity. However, since the deconvolution is performed in the Fourier domain, it implies a spatially invariant reflectivity, which is the case of horizontal reflector in constant velocity medium. Thus it has a disadvantage that is difficulty in implementing.

Imaging condition in planewave synthesis migration

In planewave synthesis imaging, the deconvolution of the downgoing wavefield from the upcoming wavefield is performed in the space domain as profile imaging does. As explained in an earlier section, the deconvolution in the space domain implies diagonality of reflectivity matrix and the diagonal property is valid only if the source wave acts like a planewave locally. This is the case of planewave synthesis migration because it synthesizes a planewave source along the reflector before migration. Therefore, in planewave synthesis migration, we retrieve the angle-dependent reflectivity by using a conventional imaging condition.

COMPARISONS WITH A SIMPLE EXAMPLE

For the purposes of the comparison, let us consider the simple acoustic subsurface model shown in Figure 3a. Figure 3b displays the simulated seismic response of one shot record and shows AVO effect clearly.

To obtain the angle-dependent reflectivity with conventional prestack imaging, I applied shot profile imaging with phase-shift extrapolation, acquired the offset-dependent reflectivity image (Figure 4a), and transformed it to angle-dependent reflectivity image (Figure 4b) using the incidence angle to each depth location. Figure 5 shows an angle-dependent reflectivity image obtained using de Bruin's imaging condition; Figure 6, one obtained using planewave synthesis imaging. All of them retrieve the general amplitude increasing pattern with respect to the incidence angle. To see the amplitude more clearly, I picked amplitude of each reflectivity image at the reflector depth and plotted the amplitude as a function of the incidence angles (Figure 7). It shows the reflectivity obtained by the planewave synthesis is more close to the theoretical solution.

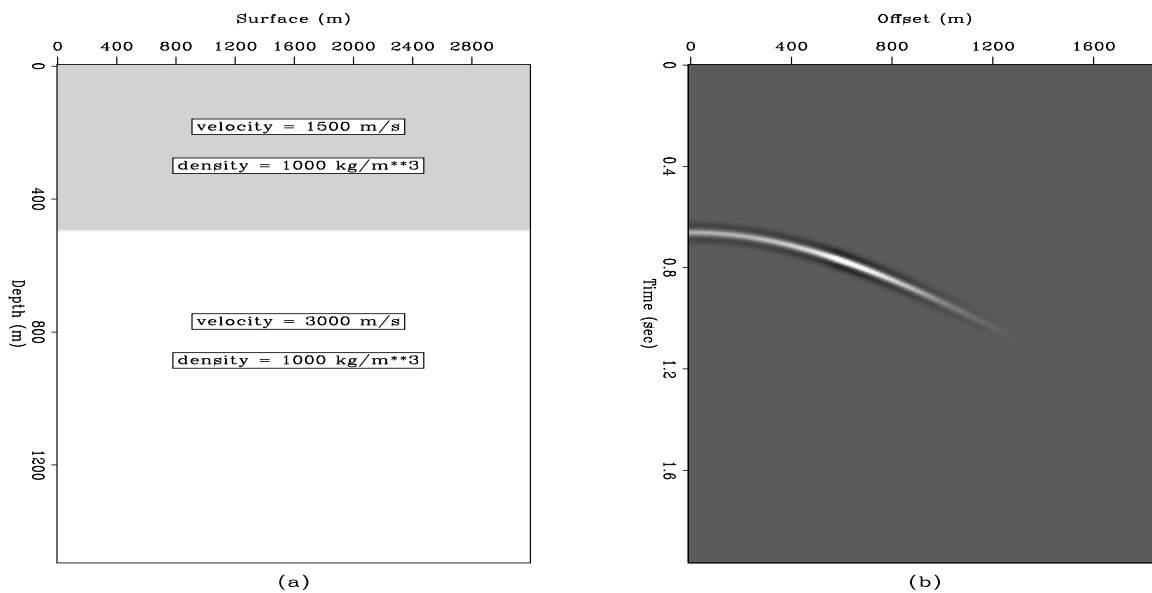


Figure 3: (a): Subsurface model of a horizontally layered acoustic medium, containing one reflector at depth $z = 500m$. (b): Simulated seismic response from the acoustic model. `jun1-modl-shot` [ER]

CONCLUSIONS

Although the imaging condition in planewave synthesis imaging is equivalent to that of conventional profile imaging, planewave synthesis imaging recover full reflectivity matrix as de Bruin's imaging condition. This is achieved due to the property of the source wavefield synthesized. Thus planewave synthesis imaging is a promising method to recover angle-dependent

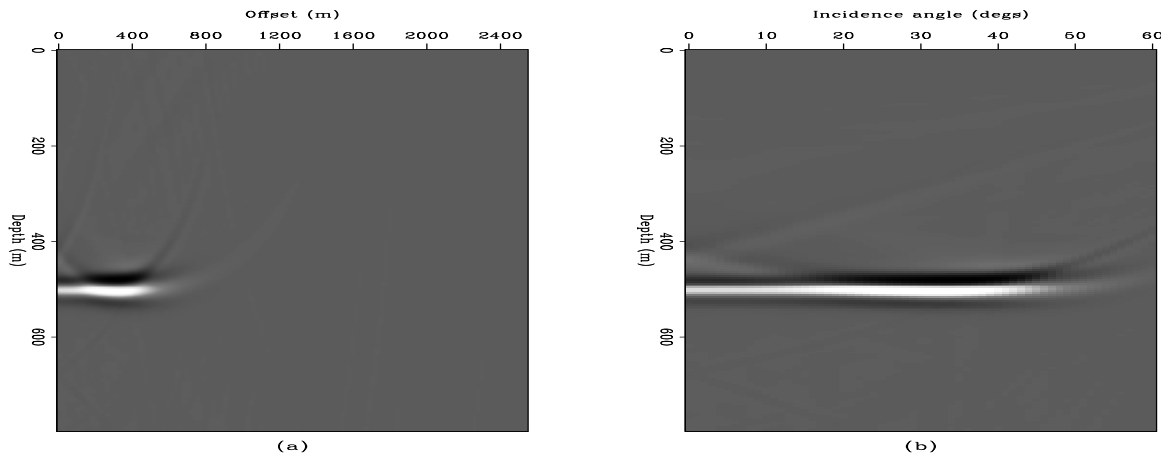


Figure 4: Offset-dependent (a) and angle-dependent (b) reflectivity image obtained by profile imaging with the conventional imaging condition. `jun1-prf-img` [ER]

Figure 5: Angle-dependent reflectivity image obtained by profile imaging with de Bruin's imaging condition. `jun1-prf-db-img` [ER]

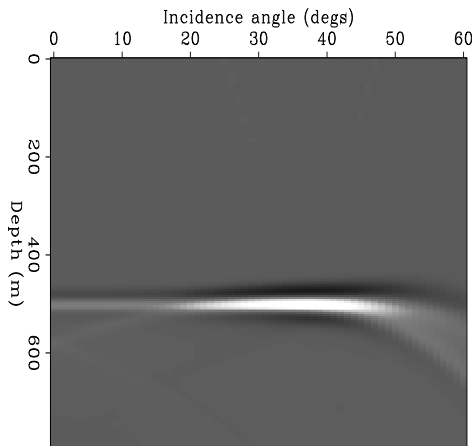


Figure 6: Angle-dependent reflectivity image obtained by the planewave synthesis imaging. `jun1-pws-img` [CR]

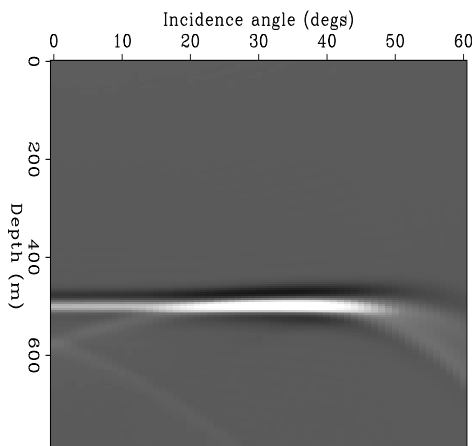
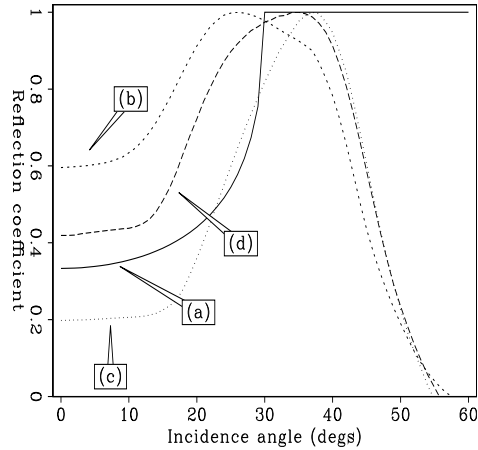


Figure 7: Angle-dependent reflection coefficient as a function of the angle of incidence: (a) the theoretical result, (b) the result of profile imaging with conventional imaging condition, (c) the result of profile imaging with de Bruin's imaging condition, and (d) the result of planewave synthesis imaging. jun1-ava [ER]



reflectivity for a nonflat reflector when lateral velocity changes. A test to a simple synthetic data showed that planewave synthesis imaging among three imaging techniques provide the closest result to the theoretical solution.

REFERENCES

- Berkhout, A. J., 1985, *Seismic migration: Imaging of acoustic energy by wave field extrapolation*: Elsevier, Amsterdam.
- Claerbout, J. F., 1985, *Imaging the Earth's Interior*: Blackwell Scientific Publications.
- de Bruin C. P. A. Wapenaar A. J. Berkhout, C. G. M., 1990, Angle-dependent reflectivity by means of prestack migration: *Geophysics*, **55**, no. 9, 1223–1234.
- Ji, J., 1993, Controlled illumination by wavefront synthesis: *SEP-79*, 129–144.
- Stoffa, P. L., and Fokkema, J. T., 1990, Split-step Fourier migration: *Geophysics*, **55**, no. 4, 410–421.

APPENDIX A

PROPERTY OF SPLIT-STEP FOURIER EXTRAPOLATION

Unitary versus Pseudounitary

A linear operator is called a unitary operator, if its adjoint equals to the inverse of it as follows:

$$W^* = W^{-1}. \quad (\text{A-1})$$

The unitary operator has the property that each eigenvalue of it is on the unit circle in complex plane.

$$W = Q \Lambda Q^* \quad (\text{A-2})$$

with $|\Lambda| = I$. Pseudounitary is a property that is closely related to the unitary. The adjoint of a pseudounitary operator is not the inverse of it.

$$W^* \neq W^{-1}. \quad (\text{A-3})$$

The pseudounitary operator, has only two kinds of eigenvalues the one that is on the unit circle in complex plane like that of unitary operator, and the other is zero. If we apply the pseudounitary forward operator followed by its adjoint operator, the resulting operator becomes idempotent operator. Therefore this property can be used as criterion for identifying a pseudounitary operator.

Split-step Fourier extrapolation operator

Split-step Fourier extrapolation (Stoffa and Fokkema, 1990) consists of two-step extrapolation, which is a phase shifting in the (k, ω) domain followed by an additional phase shifting in the (x, ω) domain. Let us consider a simple case which consist of two depth levels extrapolation. Then the forward operator can be expressed as follows:

$$W = F_t^* \exp^{-ip_1 \Delta z} F_x^* \exp^{-ip_2 \Delta z} F_x \exp^{-ip_1 \Delta z} F_x^* \exp^{-ip_2 \Delta z} F_x F_t, \quad (\text{A-4})$$

where F_x and F_t represent Fourier transform along the space and the time, respectively. The phases p_1 and p_2 quantify the amount of phase shift in the (x, ω) and in the (k, ω) domain, respectively and defined as follows:

$$p_1(x, \omega) = \omega \Delta u(x) \quad (\text{A-5})$$

and

$$p_2(k, \omega) = \omega u_0 \sqrt{1 - \left(\frac{k}{\omega u_0}\right)^2} \quad (\text{A-6})$$

where u_0 represents the reference slowness and $\Delta u(x)$ is variation of the slowness from the reference slowness. Then the adjoint of the forward operator becomes

$$W^* = F_t^* F_x^* \exp^{ip_2 \Delta z} F_x \exp^{ip_1 \Delta z} F_x^* \exp^{ip_2 \Delta z} F_x \exp^{ip_1 \Delta z} F_t. \quad (\text{A-7})$$

If we apply the adjoint operator after the forward operator as follows:

$$W^* W = F_t^* F_x^* P_2^* F_x P_1^* F_x^* P_2^* F_x P_1^* F_t F_t^* P_1 F_x^* P_2 F_x P_1 F_x^* P_2 F_x F_t \quad (\text{A-8})$$

with $P_1 = \exp^{-ip_1 \Delta z}$ and $P_2 = \exp^{-ip_2 \Delta z}$. Where P_1 is unitary operator but P_2 is pseudounitary operator because we substitute 0 for evanescent component that is the case of that p_2 becomes

imaginary. If I group the operators so that they are in the same domain, for example (k, ω) domain as follows:

$$\begin{aligned}
 W^*W &= F_t^* F_x^* (P_2^*) (F_x P_1^* F_x^*) (P_2^*) (F_x P_1^* F_t F_t^* P_1 F_x^*) (P_2) (F_x P_1 F_x^*) (P_2) F_x F_t \\
 &= F_t^* F_x^* I_p I I_p I I_p I I_p F_x F_t \\
 &= F_t^* F_x^* I_p F_x F_t
 \end{aligned} \tag{A-9}$$

where I is identity matrix and I_p is idempotent matrix with some elements are 1 and others are zeros. Therefore the split-step Fourier extrapolation is pseudounitary.

